Enhanced Efficiency of Graded-Bandgap Thin-Film Solar Cells due to Concentrated Sunlight

FAIZ AHMAD[1,2,*], AKHLESH LAKHTAKIA[2], AND PETER B. MONK[3]

[1] Department of Physics, COMSATS University Islamabad, Islamabad, Pakistan
[2] Department of Engineering Science and Mechanics, The Pennsylvania State University, University Park, PA 16802, USA
[3] Department of Mathematical Sciences, University of Delaware, Newark, DE 19716, USA
[*] Corresponding author: faizahmad@comsats.edu.pk

Compiled November 18, 2021

A systematic study was performed with a coupled optoelectronic model to examine the effect of the concentration of sunlight on the efficiencies of CIGS, CZTSSe, and AlGaAs thin-film solar cells with a graded-bandgap absorber layer. An efficiency of 34.6% for CIGS thin-film solar cells and an efficiency of 29.9% for CZTSSe thin-film solar cells are predicted with a concentration of one hundred suns, the respective one-sun efficiencies being 27.7% and 21.7%. An efficiency of 36.7% is predicted for AlGaAs thin-film solar cells with a concentration of sixty suns, in comparison to 34.5% one-sun efficiency. Sunlight concentration does not affect the per-sun electron-hole-pair (EHP) generation rate but reduces the per-sun EHP recombination rate either near the front and back faces or in the graded-bandgap regions of the absorber layer, depending upon the semiconductor used for that layer, and this is the primary reason for the improvement in the efficiency. Other effects include the enhancement of open-circuit voltage which can be positively correlated to the higher short-circuit current density. Sunlight concentration can therefore play a significant role in enhancing the efficiency of thin-film solar cells.

OCIS codes: (350.650) Solar energy; (310.0310) Thin films; (130.5990) Semiconductors.

http://dx.doi.org/10.1364/ao.XX.XXXXXX

1. INTRODUCTION

There has been increasing interest in solar photovoltaic (PV) technology in the last two decades, especially to increase the power-conversion efficiency and to reduce the levelized cost of electricity (LCOE) generated by solar PV modules. Although these modules outperform conventional sources in LCOE [1] in some geographical areas, a further cost reduction will make them globally competitive with conventional sources and allow us to better tackle the climate emergency [2].

One method to improve the efficiency and thereby reduce the LCOE is to use optical concentrators to increase the intensity of sunlight incident on the solar cell's surface. Concentrated photovoltaic (CPV) systems occupy a smaller area and use less photon-absorbing semiconductor material in comparison to the conventional non-CPV systems [3]. However, CPV systems typically use more sophisticated and expensive multi-junction solar cells [3], the most efficient of which contain III-V semiconductors. The current record efficiency of 47.1% was established with a concentration of 143 suns [4, 5].

Unfortunately, III-V multi-junction solar cells are expensive because they (i) use scarce materials and (ii) require time-consuming and expensive manufacturing processes such as metal-organic vapor-phase epitaxy [6]. Furthermore, these solar cells contain expensive substrates such as Ge, GaAs, and InP wafers [6]. Finding a suitable CPV system that requires only Earth-abundant (and therefore cheap) semiconductors and inexpensive substrates, and can be manufactured using low-cost processes, is the key challenge for CPV technology. Moreover, with the increased interest in integrating CPV systems into residential and office buildings [7–10], bringing down their LCOE is necessary to make them competitive with non-CPV systems.

The most expensive component of a CPV system is the solar cell itself [11]; so, decreasing the cost of the solar cell is crucial. Single-junction thin-film solar cells are cheap and easy to manufacture. However, the efficiencies of these solar cells are lower than of multi-junction III-V thin-film solar cells [5]. The incorporation of standard thin-film solar cells in CPV systems will therefore reduce efficiency. That reduction can be offset by concentrating sunlight more but with costly optics that would render the CPV systems commercially unviable.

Theoretical studies have shown that bandgap grading of the main photon-absorbing semiconductor layer can significantly improve the efficiency of thin-film solar cells [12–18], and this idea has been backed by simple experimental studies with bandgap grading achieved through compositional grading

possible in compound semiconductors [19–21]. CIGS [12, 13], CZTSSe [15, 16], and AlGaAs [18] thin-film solar cells with graded-bandgap absorbing layers have been theoretically predicted to deliver one-sun efficiencies as high as 27.7%, 21.7%, and 34.5%, respectively, whereas the best conventional crystalline-silicon solar cell has a one-sun efficiency of 26.7% [5, 6]. The massive efficiency gains arise because bandgap grading can provide a way to capture solar photons in a wider spectral regime, which is also the principle exploited in multi-junction III-V solar cells. Moreover, bandgap grading provides additional benefits of a higher open-circuit voltage and reduced parasitic impedances, without the additional circuitry needed for multi-junction solar cells [6]. Hence, optical concentration combined with bandgap grading of thin-film solar cells may offer a cost-effective alternative to III-V multi-junction solar cells.

In this paper, we present the results of a systematic computational study to examine the effects of concentrated sunlight on the efficiencies of thin-film solar cells with a graded-bandgap absorber layer. Three different types of thin-film solar cells—CIGS, CZTSSe, and AlGaAs—were considered, as these are widely investigated thin-film solar cells with the absorber layer made of a compound semiconductor. A coupled optoelectronic model [22–24] and the differential evolution algorithm (DEA) [25] were used together to maximize the efficiency η against the bandgap-grading parameters [24] and the sunlight-concentration factor c_{sun}. The bandgap of the absorber layer in each thin-film solar cell was considered to be nonlinearly graded along the thickness direction. Since the thickness of thin-film solar cells is on the order of a few micrometers, $c_{\text{sun}} \in [1, 100]$ was restricted to be of medium magnitude in order to avoid detrimental heating effects. Furthermore, a detailed study was performed to understand the physical reasons for efficiency improvement due to sunlight concentration.

The theoretical results presented are based on a two-step optoelectronic model [22–24]. In the optical step of this model, the transfer-matrix method [26, 27] is used for CIGS and CZTSSe solar cells to determine the electron-hole-pair (EHP) generation rate G inside the solar cell [12, 13], assuming normal illumination by unpolarized polychromatic light endowed with the AM1.5G solar spectrum [28]. The rigorous coupled-wave approach (RCWA) [24, 27] is used for the AlGaAs thin-film solar cells as it involves localized Pd-Ge-Au ohmic back-contacts embedded periodically in an Ag backreflector (grating) [18, 27, 29]. The transfer-matrix method is an efficient technique to compute the reflectances, transmittances, and absorptances of a multilayered structure with a plane-stratified morphology, as shown in Fig. 1(a) for the CIGS and CZTSSe solar cells. But the transfer-matrix method is inapplicable to the AlGaAs solar cell, shown in Fig. 1(b), since it contains a grating, and the RCWA has to be used.

In the electrical step of the model, G appears as a forcing function in the system of one-dimensional (1D) drift-diffusion equations applied to the semiconductor portion of the solar cell [30]. These equations are solved using a hybridizable discontinuous Galerkin scheme [31–33] to determine the device current density J_{dev} and the electrical power density P as functions of the external bias voltage V_{ext} [24]. The coupled optoelectronic model has been validated against several experimental results on solar cells with a homogeneous-bandgap absorber layer [12, 13, 15, 16, 18].

The structure of this paper is as follows. Section 2 contains brief descriptions of the chosen thin-film solar cells as well as the coupled optoelectronic model. Section 3.A presents data on performance predicted for CIGS solar cells, Sec. 3.B on CZTSSe solar cells, and Sec. 3.C on AlGaAs solar cells, for $c_{\text{sun}} \in [1, 100]$. The detailed study of underlying physics to improve the efficiency of solar cells by concentrating sunlight is discussed in Sec. 3.D. Some remarks in Sec. 4 conclude this paper.

2. OPTOELECTRONIC CALCULATIONS

The structures of the standard CIGS and CZTSSe thin-film solar cells are the same except that the CIGS layer is replaced with the CZTSSe layer, as shown in Fig. 1(a). Detailed geometrical, optical, and electronic descriptions of these solar cells are available elsewhere [12, 13, 15, 16, 24]. A brief review is as follows. The standard CIGS (CZTSSe) solar cell has a MgF_2/AZO/od-ZnO/CdS/CIGS (CZTSSe)/Al_2O_3/Mo multilayered structure [shown in Fig. 1(a)], with magnesium fluoride (MgF_2) as an antireflection coating [34], aluminum-doped zinc oxide (AZO) as the front-contact layer to collect electrons [35], oxygen-deficient zinc oxide (od-ZnO) [36] and cadmium sulfide (CdS) [37] together forming a bilayer buffer that also serves as an n-type semiconductor, a p-type CIGS (CZTSSe) photon-absorbing layer, aluminum oxide (Al_2O_3) [38] as back-surface passivation layer, and molybdenum (Mo) [39] as the back-contact layer to collect holes as well as to serve as an optical reflector. The typical thicknesses of all the layers in Fig. 1(a) are as follows: $L_{\text{ARC}} = 110$ nm (MgF_2), $L_{\text{TCO}} = 100$ nm (AZO), $L_{\text{FSP}} = 80$ nm (od-ZnO), $L_{\text{w}} = 70$ nm (CdS), $L_{\text{s}} = 2200$ nm (CIGS or CZTSSe), $L_{\text{BSP}} = 20$ nm (Al_2O_3), and $L_{\text{Mo}} = 500$ nm (Mo). The thickness direction is parallel to the z axis, and the solar cell is invariant along the x and y axes.

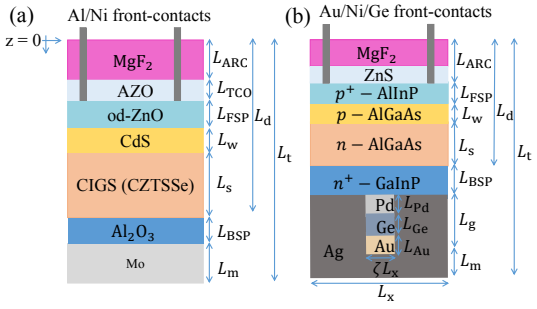

Fig. 1. Schematics of (a) CIGS or CZTSSe and (b) AlGaAs thin-film solar cells.

Detailed geometrical, optical, and electronic descriptions of the AlGaAs solar cell are available elsewhere [18, 24]; however, a brief review is as follows. The standard AlGaAs thin-film solar cell has the MgF_2/ZnS/AlInP/p-AlGaAs/n-AlGaAs/GaInP/Pd-Ge-Au multilayered structure, with $\zeta = 1$ and $L_{\text{m}} = 0$ in Fig. 1(b). Together, an MgF_2 layer on top of a zinc sulfide (ZnS) layer constitute an antireflection coating. Heavily doped aluminum-indium phosphide (p^+-AlInP) is used as the front-surface passivation layer as well as the front-contact layer. The p-type AlGaAs works as a emitter layer, followed by the main photon-absorbing layer made of n-type AlGaAs. Heavily doped gallium-indium phosphide (n^+-GaInP) plays the role of back-surface passivation layer. The back electrode commonly used in thin-film GaAs solar cells is a palladium-germanium-gold (Pd-Ge-Au) trilayer, which is neither periodic ($\zeta = 1$) nor backed by an Ag layer ($L_{\text{m}} = 0$). However, we have utilized the idea of localized ohmic back-contacts by using the Ag/Pd-Ge-Au periodic structure with $\zeta \in (0, 1)$ and $L_{\text{m}} > 0$ in Fig. 1(b),

the Pd-Ge-Au trilayered segments for better charge-carrier collection, and the Ag layer for better optical reflection [29]. The total thickness of the Pd-Ge-Au trilayer is $L_g = 170$ nm and its width is $\zeta L_x \in (0, L_x)$, where $L_x \leq 1000$ nm is the period along the x axis. The thicknesses of the individual layers in the trilayer are: $L_{Pd} = 20$ nm (Pd), $L_{Ge} = 50$ nm (Ge), and $L_{Au} = 100$ nm (Au). The typical thicknesses of all other layers in Fig. 1(b) are as follows: $L_{ARC} = 260$ nm due to an MgF_2 layer of 110 nm and a ZnS layer of 150 nm, $L_{FSP} = 20$ nm (p^+-AlInP), $L_w = 50$ nm (p-AlGaAs), $L_s = 2000$ nm (n-AlGaAs), $L_{BSP} = 20$ nm (n^+-GaInP), and $L_m = 100$ nm (Ag). The solar cell is invariant along the y axis.

The nonlinearly graded bandgap energy of the absorber layer was taken to be [24]

$$\mathsf{E}_g(z) = \mathsf{E}_a + A\,(\mathsf{E}_b - \mathsf{E}_a) \times \left[\frac{1}{2}\left(\sin\left\{2\pi\left[K\frac{z-(L_d-L_s)}{L_s} - \nu\right]\right\} + 1\right)\right]^{\alpha}, \quad z \in (L_d - L_s, L_d)\,, \tag{1}$$

where E_a is the minimum bandgap energy, E_b is the maximum bandgap energy, A is an amplitude (with $A = 0$ representing a homogeneous layer), $\nu \in [0,1)$ quantifies a relative phase shift, $\alpha > 0$ is a shaping parameter, and $K \geq 0$ is a cycle number that need not be an integer. The solar cell was taken to be illuminated from the front by sunlight from c_{sun} suns, the solar irradiance from each having the standard AM1.5G spectrum [28].

The optical calculations for CIGS and CZTSSe solar cells were performed using the transfer-matrix method [26, 27], with the optical data for all materials collected from many sources [34–42]. The EHP generation rate $G(z)$ obtained from the optical step was then used as an input to the electrical step [24], with electrical data for all materials collected from diverse sources [43–45].

The optical calculations for AlGaAs solar cells were performed using the RCWA [24, 46] to determine the EHP generation rate $G(x,z) = G(x \pm L_x, z)$, the simple transfer-matrix method [26, 27] being inadequate to account for the nonspecular diffraction effects produced by the structural periodicity of the Ag/Pd-Ge-Au backside. The optical data for all materials in the AlGaAs solar cells were taken from standard sources [34, 39, 47–51]. Since L_x is much smaller than the transverse dimensions of the solar cell, $G(x,z)$ was averaged over one period along the x axis to calculate $G(z)$. The electrical data needed for all materials in the solar cell are available elsewhere [18, 24, 52–56].

After the 1D drift-diffusion equations [30] have been solved for a fixed value of the bias voltage V_{ext} in the electrical step, the outputs are the device current density J_{dev} and the electrical power density P. The J_{dev}-V_{ext} curve and the P-V_{ext} curve yield the short-circuit current density J_{sc}, the open-circuit voltage V_{oc}, and the power-conversion efficiency η. The fill factor FF is calculated as $P_{max}/J_{sc}V_{oc}$.

The DEA [25] was used to maximize η with respect to c_{sun} and the bandgap parameters appearing on the right side of Eq. (1).

3. NUMERICAL RESULTS AND DISCUSSIONS

A. CIGS solar cell

First, we considered the optoelectronic optimization of η of the CIGS thin-film solar cell with a graded-bandgap CIGS absorber layer of 2200-nm thickness. With $\mathsf{E}_b = 1626$ meV in Eq. (1) fixed, the six-dimensional parameter space for optimization of η was as follows: $c_{sun} \in [1,100]$, $\mathsf{E}_a \in [947,1626]$ meV, $A \in [0,1]$, $\alpha \in [0,8]$, $K \in [0,8]$, and $\nu \in [0,1]$.

The model predicted one-sun (i.e., $c_{sun} = 1$) values of η, J_{sc}, V_{oc}, and FF are 27.67%, 33.16 mA cm^{-2}, 1070 mV, and 78%, respectively [12, 13]. The corresponding bandgap-grading parameters are: $\mathsf{E}_a = 950$ meV, $A = 0.99$, $\alpha = 6$, $K = 1.5$, and $\psi = 0.75$. The efficiency continued to rise monotonically as c_{sun} increased, the maximum η predicted being 34.63% with $c_{sun} = 100$. The corresponding values of J_{sc}, V_{oc}, and FF are 3692 mA cm^{-2}, 1174 mV, and 80%, respectively. The bandgap-grading parameters remain unchanged with higher sunlight concentration.

A relative enhancement of 25.15% in η is predicted with 100-sun concentration over the one-sun efficiency. The huge increase in J_{sc} with sunlight concentration is directly related to the higher EHP generation rate with sunlight concentration, and V_{oc} is also improved thereby because it is proportional to $\ln(1 + J_{sc}/J_{dark})$ for ideal photodiodes, where J_{dark} is the dark current density; see Eq. (1.6) of Ref. 30. We confirmed that η can be enhanced further with $c_{sun} > 100$, but considering the few-micrometer thickness of the CIGS solar cell, we did not pursue that avenue to avoid detrimental heating effects.

The J_{dev}-V_{ext} and P-V_{ext} characteristics of the optimal CIGS thin-film solar cell are shown in Fig. 2 for $c_{sun} \in \{1,100\}$. The maximum output power P_{max} delivered is 27.67 mW cm^{-2} for $c_{sun} = 1$ but 3463 mW cm^{-2} for $c_{sun} = 100$. Of course, the ratio P_{max}/c_{sun} increases by 25.15% with hundredfold sunlight concentration, as is expected from the increase of η by the same factor.

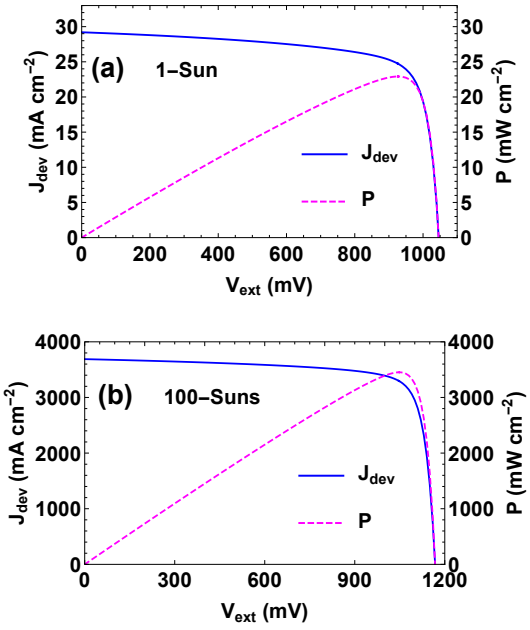

Fig. 2. Plots of J_{dev} and P vs. V_{ext} of the optimal CIGS thin-film solar cell when (a) $c_{sun} = 1$ and (b) $c_{sun} = 100$.

The plots of J_{sc}, V_{oc}, η, and FF of the optimal CIGS solar cell

as functions of $c_{sun} \in [1,100]$ are shown in Fig. 3(a)–(d). The linear relationship of J_{sc} with c_{sun} can be noted from Fig 3(a). In contrast, both V_{oc} and η show a three-phase trend: as c_{sun} increases from 1 to 100, each of V_{oc} and η increases linearly at a high rate in the first phase, then its rate of increase gradually reduces in the second phase, and finally it increases linearly at a slow rate in the third phase. However, FF is affected very little by sunlight concentration.

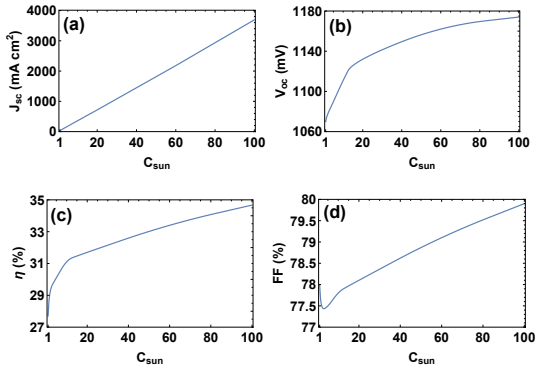

Fig. 3. Plots of (a) J_{sc}, (b) V_{oc}, (c)) η, and (d) FF of the optimal CIGS thin-film solar cell as functions of c_{sun}.

B. CZTSSe solar cell

Next, we considered the optoelectronic optimization of η of the CZTSSe solar cell with a 2200-nm-thick graded-bandgap CZTSSe absorber layer. With $E_b = 1490$ meV in Eq. (1) fixed, the six-dimensional parameter space for optimization of η was as follows: $c_{sun} \in [1,100]$, $E_a \in [910,1490]$ meV, $A \in [0,1]$, $\alpha \in [0,8]$, $K \in [0,8]$, and $\nu \in [0,1]$.

The model predicted one-sun values of η, J_{sc}, V_{oc}, and FF are 21.74%, 37.39 mA cm^{-2}, 772 mV, and 75%, respectively [18]. The corresponding bandgap-grading parameters are: $E_a = 920$ meV, $A = 0.99$, $\alpha = 6$, $K = 2$, and $\psi = 0.75$. For concentrated sunlight, the maximum η predicted is 29.93% with $c_{sun} = 100$. The corresponding values of J_{sc}, V_{oc}, and FF are 4125 mA cm^{-2}, 955 mV, and 76%, respectively. The bandgap-grading parameters for $c_{sun} = 100$ are the same as for $c_{sun} = 1$.

Thus, the 100-sun efficiency of the CZTSSe solar cell is 37.7% higher than its 1-sun efficiency. This enhancement is accompanied by a 10.3% enhancement in per-sun short-circuit current density J_{sc}/c_{sun} and a 23.7% enhancement in V_{oc}, the enhancement in J_{sc} being due to the higher EHP generation rate arising from sunlight concentration. Just as for the CIGS solar cell, we did not let c_{sun} exceed 100 to avoid excessive heating, although the predicted η would have increased further. From the J_{dev}-V_{ext} and P-V_{ext} characteristics of the CZTSSe solar cell shown in Fig. 4, the maximum output power P_{max} is 21.74 mW cm^{-2} for $c_{sun} = 1$ but 2993 mW cm^{-2} for $c_{sun} = 100$.

The relative enhancement in efficiency (37.9%) for the optimal CZTSSe solar cell with sunlight concentration is higher than the relative enhancement in efficiency (25.15%) for the optimal CIGS solar cell, although the CZTSSe solar cell is less efficient than the CIGS solar cell for $c_{sun} \in \{1,100\}$.

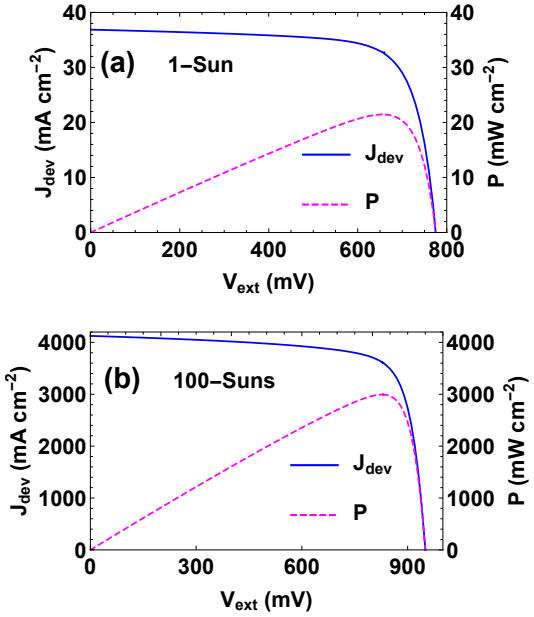

Fig. 4. Plots of J_{dev} and P vs. V_{ext} of the optimal CZTSSe solar cell (a) $c_{sun} = 1$ and (b) $c_{sun} = 100$.

The plots of J_{sc}, V_{oc}, η, and FF as functions of c_{sun} are presented in Fig. 5(a)–(d) for the optimal CZTSSe solar cell. The variations of J_{sc}, V_{oc}, and η with c_{sun} for the optimal CZTSSe solar cell are qualitatively similar to their counterparts for the optimal CIGS solar cell [Figs. 3(a)–(c)]. The variation of FF with c_{sun} is somewhat different for the two solar cells, but in practical terms the dependence of FF is weak for both solar cells.

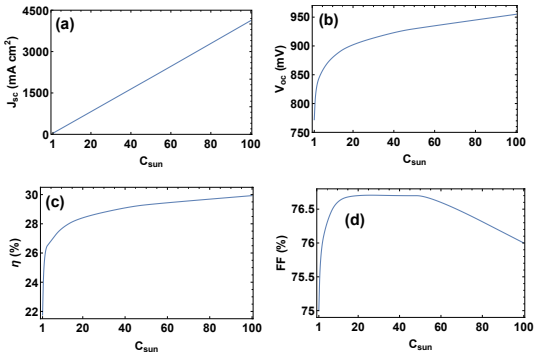

Fig. 5. Plots of (a) J_{sc}, (b) V_{oc}, (c)) η, and (d) FF of the optimal CZTSSe thin-film solar cell as functions of c_{sun}.

C. AlGaAs solar cell

Lastly, we considered the optoelectronic optimization of η of the AlGaAs thin-film solar cell with a 2000-nm-thick graded-bandgap AlGaAs absorber layer. We fixed $L_x = 500$ nm and $\zeta = 0.05$, in accordance with previous studies [18]. Also, the bandgap energies of p^+-AlInP, p-AlGaAs, n^+-GaInP were fixed at 2350 meV, 2090 meV, and 1900 meV, respectively. With E_b set equal to 2090 meV in Eq. (1), the six-dimensional parameter space for optimization of η was as follows: $c_{sun} \in [1,100]$, $E_a \in [1424,2090]$ meV, $A \in [0,1]$, $\alpha \in [0,8]$, $K \in [0,8]$, and $\nu \in [0,1]$.

The model predicted one-sun values of η, J_{sc}, V_{oc}, and FF are 34.5%, 24.8 mA cm^{-2}, 1556 mV, and 89%, respectively, the corresponding bandgap-grading parameters being $E_a = 1424$ meV,

$A = 0.99$, $\alpha = 6$, $K = 3$, and $\psi = 0.75$. Unlike for the CIGS and CZTSSe solar cells, η does not rise monotonically as $c_{\rm sun}$ increases from 1 to 100. Instead, it first increases and then decreases, the maximum η predicted being 36.7% with $c_{\rm sun} = 60$. The corresponding values of $J_{\rm sc}$, $V_{\rm oc}$, and FF are 1512 mA cm^{-2}, 1657 mV, and 88%, respectively. The bandgap-grading parameters remain unchanged with sunlight concentration.

A relative enhancement of 6.4% in η is predicted with sunlight concentration. According to the $J_{\rm dev}$-$V_{\rm ext}$ and P-$V_{\rm ext}$ characteristics shown in Fig. 6, the maximum output power delivered is 34.50 mW cm^{-2} for $c_{\rm sun} = 1$ but 2200 mW cm^{-2} for $c_{\rm sun} = 60$.

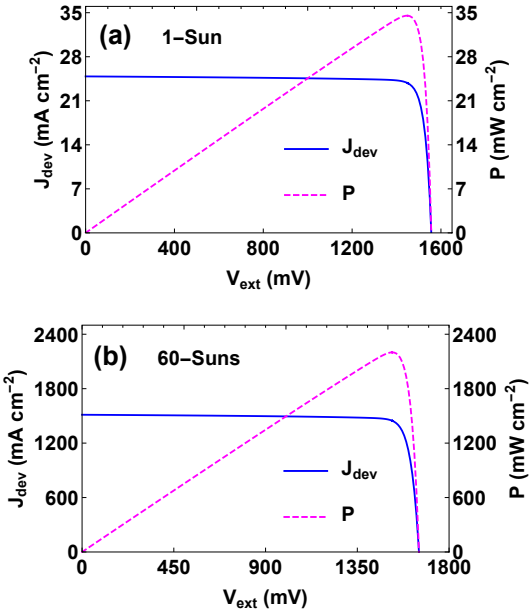

Fig. 6. Plots of $J_{\rm dev}$ and P vs. $V_{\rm ext}$ of the optimal AlGaAs thin-film solar cell when (a) $c_{\rm sun} = 1$ and (b) $c_{\rm sun} = 60$.

The plots of $J_{\rm sc}$, $V_{\rm oc}$, η, and FF as functions of $c_{\rm sun} \in [1, 100]$ are shown in Fig. 7(a)–(d) for the optimal AlGaAs solar cell. The variations of $J_{\rm sc}$ and $V_{\rm oc}$ are qualitatively similar to their counterparts for the optimal CIGS solar cell [Figs. 3(a), (b)] and the optimal CZTSSe solar cell [Figs. 5(a), (b)]. The best sunlight concentration ($c_{\rm sun} = 60$) for the optimal AlGaAs solar cell ($c_{\rm sun} = 60$) is under 100, unlike for the optimal CIGS and the optimal CZTSSe solar cells. Finally, although the dependences of FF with $c_{\rm sun}$ are not qualitatively similar for all three solar cells, but FF varies in the small range of $\pm 1.25\%$ for any of those solar cells.

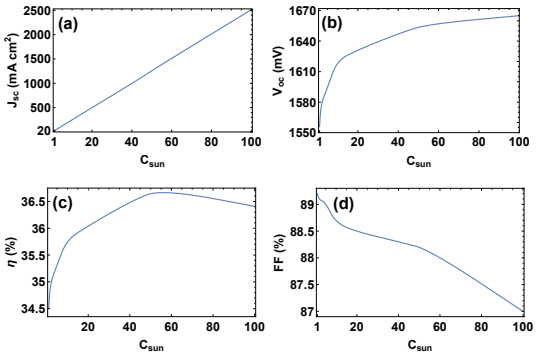

Fig. 7. Plots of (a) $J_{\rm sc}$, (b) $V_{\rm oc}$, (c)) η, and (d) FF of the optimal AlGaAs thin-film solar cell as functions of $c_{\rm sun}$.

The relative enhancement in efficiency with sunlight concentration is highest for the CZTSSe solar cell among all three types of solar cells. It is conjectured that the higher relative enhancement in η with $c_{\rm sun}$ is related to the lower bound $\mathsf{E}_{\rm a}$ of $\mathsf{E}_{\rm g}(z)$ in Eq. (1). The optimal CZTSSe solar cell has the lowest $\mathsf{E}_{\rm a}$ (920 mV) and the optimal AlGaAs solar cell has the highest $\mathsf{E}_{\rm a}$ (1424 mV) among the three solar cells. The relative enhancements in η are 37.7% (CZTSSe), 25.15% (CIGS), and 6.4% (AlGaAs). Lower values of $\mathsf{E}_{\rm a}$ will elevate the electron-hole-pair generation rate [24].

With $c_{\rm sun} \in [1, 100]$ in the parameter space chosen for optimization, both the CIGS and CZTSSe solar cells deliver maximum efficiency at $c_{\rm sun} = 100$ but the AlGaAs solar cell at $c_{\rm sun} = 60$. This diversity in the dependence of η on $c_{\rm sun}$ may be fictitious in that η is maximum at some $c_{\rm sun} > 100$ for the CIGS and CZTSSe solar cells. Or, this diversity could arise from differences in some physical mechanisms. This issue is very likely irrelevant in practical situations.

D. Effect of sunlight concentration on generation/recombination processes

Sunlight concentration is considerably more effective in raising the efficiencies of the optimal CIGS and CZTSSe solar cells than of the optimal AlGaAs solar cell, as is clear from Table I. Whereas $J_{\rm sc}/c_{\rm sun}$ is enhanced approximately the same for both the CIGS and CZTSSe solar cells, $V_{\rm oc}$ enhancement for the CZTSSe solar cell is more than twice of the CIGS solar cell. This is the reason why efficiency enhancement is higher for the CZTSSe solar cell than for the CIGS solar cell.

Enhancements of both $J_{\rm sc}/c_{\rm sun}$ and $V_{\rm oc}$ due to sunlight concentration are significantly smaller for the AlGaAs solar cell than for the other two solar cells. Especially, the enhancement of $J_{\rm sc}/c_{\rm sun}$ is very modest (1.6%) for the AlGaAs solar compared to the CIGS and CZTSSe solar cells. Since $V_{\rm oc}$ is proportional to $\ln(1 + J_{\rm sc}/J_{\rm dark})$ for ideal photodiodes, the processes of generation and recombination of electrons and holes must be responsible for both (i) efficiency enhancement on sunlight concentration and (ii) the greater effectiveness of sunlight concentration for CIGS and CZTSSe solar cells than for the AlGaAs solar cell.

All materials inside a solar cell are optically characterized as linear materials described by a relative permittivity that is independent of the magnitudes of the electric and magnetic fields. As the absorption rate of the monochromatic optical energy per unit volume is proportional to the square of the magnitude of the electric field [57], the number density of photons of a certain free-space wavelength absorbed in an elementary volume in any

Table I. Percent increases of η, J_{sc}/c_{sun}, and V_{oc} upon sunlight concentration.

Solar cell	c_{sun} for max η	Increase in η	Increase in J_{sc}/c_{sun}	Increase in V_{oc}
CIGS	100	25.1%	11.3%	9.7%
CZTSSe	100	37.9%	10.3%	23.7%
AlGaAs	60	6.4%	1.6%	6.5%

layer in a solar cell is linearly proportional to the intensity of that spectral component of the incident sunlight. If $G_{c_{sun}}(z)$ denotes the c_{sun}-sun generation rate, then

$$G_{c_{sun}}(z) = c_{sun}\, G_1(z)\,. \tag{2}$$

In contrast, the radiative, Shockley–Read–Hall, and Auger components of the electron-hole recombination rate depend nonlinearly on the electron and hole densities, as does charge-carrier transport [24, 30]. Therefore, if $R_{c_{sun}}(z)$ denotes the recombination rate in relation to c_{sun}, then

$$R_{c_{sun}}(z) \neq c_{sun}\, R_1(z) \tag{3}$$

in general.

It follows from Eqs. (2) and (3) that, while the spatial profiles of $G_1(z)$ and $G_{c_{sun}}(z)/c_{sun}$ must be identical, the spatial profiles of $R_1(z)$ and $R_{c_{sun}}(z)/c_{sun}$ may well be different. We examined these spatial profiles in order to determine which portions of the semiconductor region are responsible for efficiency enhancement from sunlight concentration. We also determined the values of the net generation rate $\gamma_{c_{sun}}$ and the net recombination rate $\rho_{c_{sun}}$, which are the integrals of $G_{c_{sun}}(z)$ and $R_{c_{sun}}(z)$, respectively, over the semiconductor region of each solar cell.

D.1. CIGS solar cells

The EHP generation rates $G_{100}(z)$ and $100\,G_1(z)$ are plotted as functions of z in the semiconductor region of the optimal CIGS solar cell in Fig. 8(a). The plots show that $G_{100}(z) = 100\,G_1(z)$, as expected from Eq. (2). Not surprisingly therefore, $\gamma_{100} = 100\gamma_1 = 2.66 \times 10^{26}$ cm^{-2} s^{-1}.

The EHP recombination rates $R_{100}(z)$ and $100R_1(z)$ are plotted as functions of z in the semiconductor regions of the same solar cell in Fig. 8(b). The truth of the inequality (3) is evidenced by the plots. Note that $R_{100}(z) < 100R_1(z)$ in most of the CIGS layer, but the per-sun recombination rate near the two faces of that layer is affected very little by sunlight concentration. In consequence of $100R_1(z)$ exceeding $R_{100}(z)$ significantly in most of the CIGS layer, $100\rho_1 = 6.21 \times 10^{25}$ cm^{-2} s^{-1} is 164% higher than $\rho_{100} = 2.35 \times 10^{25}$ cm^{-2} s^{-1}, which shows that the reduced per-sun recombination rate is the major reason for the efficiency enhancement in the CIGS solar cell on exposure to concentrated sunlight.

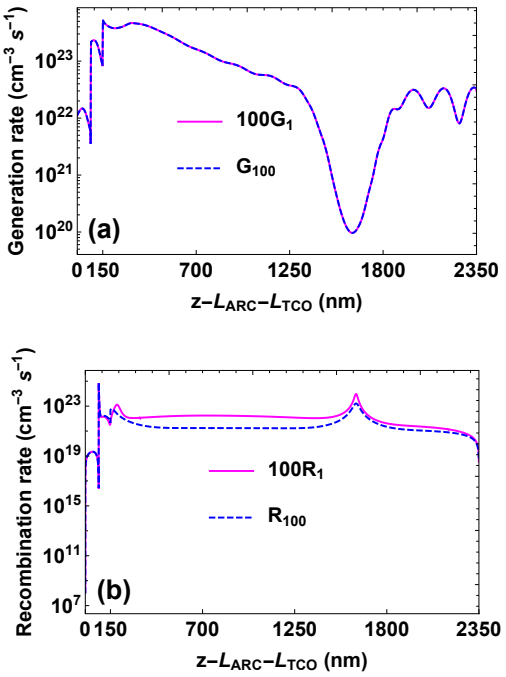

Fig. 8. Spatial profiles of (a) the EHP generation rate and (b) the EHP recombination rate in the semiconductor region of the optimal CIGS solar cell, for the one-sun and 100-sun illumination conditions.

D.2. CZTSSe solar cells

The EHP generation rates $G_{100}(z)$ and $100\,G_1(z)$ are plotted as functions of z in the semiconductor regions of the optimal CZTSSe solar cell in Fig. 9(a). The plots show that $G_{100}(z) = 100\,G_1(z)$, as expected from Eq. (2); also, $\gamma_{100} = 100\gamma_1 = 2.79 \times 10^{26}$ cm^{-2} s^{-1}.

In contrast to the CIGS solar cell, the generation rates $R_{100}(z)$ and $100R_1(z)$ in Fig. 9(b) are almost the same inside the CZTSSe solar cells except in the vicinity of the CdS/CZTSSe interface. Consistently, with that observation, $100\rho_1 = 3.73 \times 10^{25}$ cm^{-2} s^{-1} is 6% lower than $\rho_{100} = 3.97 \times 10^{25}$ cm^{-2} s^{-1}. However, the improvement in efficiency can be correlated with (i) the lowered per-sun recombination rate near the CdS/CZTSSe interface that would improve carrier collection and (ii) the significantly higher V_{oc} due to larger J_{sc} [30].

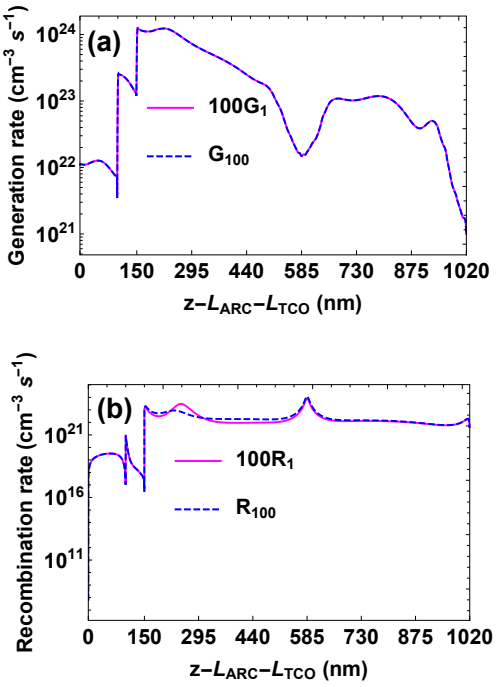

Fig. 9. Spatial profiles of (a) the EHP generation rate and (b) the EHP recombination rate in the semiconductor region of the optimal CZTSSe solar cell, for the one-sun and 100-sun illumination conditions.

D.3. AlGaAs solar cells

Figure 10(a) shows the spatial profiles $G_{60}(z)$ and $60\,G_1(z)$ in the semiconductor region of the optimal AlGaAs solar cell. As expected, $G_{60}(z) = 60\,G_1(z)$; we also found that $\gamma_{60} = 60\gamma_1 = 1.08 \times 10^{26}$ cm^{-2} s^{-1}. The per-sun generation rate in the optimal AlGaAs solar cell is about two-thirds of its counterparts in the other two optimal solar cells (see Table II), because

(a) the minimum bandgap energy of AlGaAs (1424 meV) is considerably larger than the minimum bandgap energies of CIGS (947 meV) and CZTSSe (910 meV) and

(b) the maximum bandgap energy of AlGaAs (2090 meV) is considerably larger than the minimum bandgap energies of CIGS (1626 meV) and CZTSSe (1490 meV).

A lower bandgap energy makes it easier for electrons to move from the valence band to the conduction band. However, the optimal AlGaAs solar cell is more efficient than the other two types of optimal solar cells because V_{oc} is higher for the former than for the latter two.

The spatial profiles of $R_{60}(z)$ and $60R_1(z)$ in Fig. 10(b) clearly show that $R_{60}(z) \neq 60R_1(z)$ in the semiconductor region of the AlGaAs solar cell. Although $R_{60}(z) < 60R_1(z)$ in the vicinity of the front and back interfaces of the AlGaAs absorber layer, the recombination rate in some regions of the AlGaAs layer is a bit higher due to sunlight concentration. However, $60\rho_1 = 5.08 \times 10^{23}$ cm^{-2} s^{-1} is 73.9% higher than $\rho_{60} = 2.92 \times 10^{23}$ cm^{-2} s^{-1}, indicating that the reduced per-sun recombination rate is the major reason for the efficiency enhancement on exposure of the AlGaAs solar cell to concentrated sunlight.

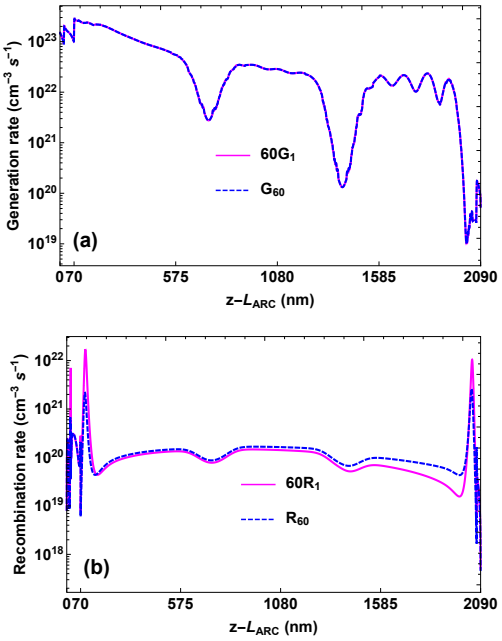

Fig. 10. Spatial profiles of (a) the EHP generation rate and (b) the EHP recombination rate in the semiconductor region of the optimal AlGaAs solar cell, for the one-sun and 60-sun illumination conditions.

According to Table II, $\gamma_{c_{sun}}/c_{sun} > \rho_{c_{sun}}/c_{sun}$ for all three types of optimal solar cells, as indeed must be expected of any electrical source. The recombination rate as a fraction of the generation rate is much smaller for the optimal AlGaAs solar cell than for the optimal CIGS and optimal CZTSSe solar cells, whether sunlight is concentrated or not, which makes the former the least wasteful of the electron-hole pairs generated in it. However, the excess per-sun generation rate $(\gamma_{c_{sun}} - \rho_{c_{sun}})/c_{sun}$ in the optimal AlGaAs solar cell is definitely smaller than in the two other two optimal solar cells, which is reflected in the per-sun short-circuit current density J_{sc}/c_{sun} being the smallest for the optimal AlGaAs solar cell. However, both V_{oc} and FF are much larger for the optimal AlGaAs solar cell than for the other two optimal solar cells, overcompensating for the lowest J_{sc}/c_{sun} to result in the highest value of η for the optimal AlGaAs solar cell.

Table II. Efficiency, per-sun EHP generation rate, and per-sun EHP recombination rate in relation to the number of suns. Both rates are in units of 10^{23} cm^{-2} s^{-1}.

Optimal solar cell	η			$\gamma_{c_{\rm sun}}/c_{\rm sun}$	$\rho_{c_{\rm sun}}/c_{\rm sun}$		
	$c_{\rm sun}=1$	$c_{\rm sun}=60$	$c_{\rm sun}=100$		$c_{\rm sun}=1$	$c_{\rm sun}=60$	$c_{\rm sun}=100$
CIGS	27.67%	33.41%	34.63%	26.6	6.21	2.74	2.35
CZTSSe	21.74%	29.44%	29.93%	27.9	3.73	3.95	3.97
AlGaAs	34.50%	36.67%	36.41%	18.0	0.0846	0.0486	0.0500

4. CONCLUDING REMARKS

A systematic study was performed with the coupled opto-electronic model to examine the effect of the concentration of sunlight on the efficiencies of CIGS, CZTSSe, and AlGaAs thin-film solar cells with a graded-bandgap absorber layer. An efficiency of 34.6% for the optimal CIGS solar cell and an efficiency of 29.9% for the optimum CZTSSe solar cell are predicted with a concentration of hundred suns, the respective one-sun efficiencies being 27.7% and 21.7%. An efficiency of 36.67% is predicted for the optimal AlGaAs thin-film solar cell with a concentration of sixty suns, in contrast to 34.5% one-sun efficiency.

Reduction of the recombination rates near the faces of the absorber layer in the CZTSSe and AlGaAs solar cells plays a vital role in efficiency enhancement due to concentrated sunlight; in contrast, reduction of the recombination rate inside the absorber layer plays the key role in improving the efficiency of the CIGS solar cell. Since recombination mechanisms vary from semiconductor to semiconductor, investigation of the spatial profile of the recombination rate is necessary to optimize the performance of the solar cell chosen for a CPV system. Enhancement of the open-circuit voltage of thin-film solar cells of all three types can be correlated to the higher short-circuit current density arising from concentrated sunlight.

Funding. The research of F. Ahmed and A. Lakhtakia was partially supported by US National Science Foundation (NSF) under grant number DMS-2011996. The research of P.B. Monk was partially supported by the same foundation under grant number DMS-2011603.

Acknowledgment. A. Lakhtakia thanks the Charles Godfrey Binder Endowment at the Pennsylvania State University for ongoing support of his research endeavors.

Disclosures. The authors declare no conflicts of interest.

REFERENCES

1. M. Roser, Why did renewables become so cheap so fast?, Our World in Data (2020) (accessed on October 26, 2021).
2. P. Hawken (ed.), *Drawdown: The Most Comprehensive Plan Ever Proposed to Reverse Global Warming* (Penguin, 2017).
3. F. Dimroth, T. N. D. Tibbits, M. Niemeyer, F. Predan, P. Beutel, C. Karcher, E. Oliva, G. Siefer, D. Lackner, P. Fuß-Kailuweit, A. W. Bett, R. Krause, C. Drazek, E. Guiot, J. Wasselin, A. Tauzin, and T. Signamarcheix, "Four-junction wafer-bonded concentrator solar cells," *IEEE J. Photovolt.* **6** 343–349 (2016).
4. J. F. Geisz, R. M. France, K. L. Schulte, M. A. Steiner, A. G. Norman, H. L. Guthrey, M. R. Young, T. Song, and T. Moriarty, "Six-junction III-V solar cells with 47.1% conversion efficiency under 143 Suns concentration," *Nat. Energy* **5**, 326–335 (2020).
5. National Renewable Energy Laboratory, Best Research-Cell Efficiency Chart (accessed on October 26, 2021)
6. M. A. Green, "Photovoltaic technology and visions for the future," *Prog. Energy* **1**, 013001 (2019).
7. G. Li, Q. Xuan, M. W. Akram, A. Y. Golizadeh, H. Liu, and S. Shittu, "Building integrated solar concentrating systems: A review," *Appl. Energy* **260**, 114288 (2020).
8. J. Marín-Sáez, D. Chemisana, J. Atencia, and M.-V. Collados, "Outdoor performance evaluation of a holographic solar concentrator optimized for building integration," *Appl. Energy* **250**, 1073–1084 (2019).
9. J. Day, S. Senthilarasu, and T. K. Mallick, "Enhanced efficiency for building integrated concentrator photovoltaic modules based on rare earth doped optics," *Sol. Energy Mater. Sol. Cells* **199**, 83–90 (2019).
10. Q. Xuan, G. Li, Y. Lu, X. Zhao, Y. Su, J. Ji, and G. Pei, "A general optimization strategy for the annual performance enhancement of a solar concentrating system incorporated in the south-facing wall of a building." *Indoor Built Environ.* **29**, 1386–1398 (2020).
11. International Energy Agency, *Trends in Photovoltaic Applications 2020* (accessed on August 26, 2021).
12. F. Ahmad, T. H. Anderson, P. B. Monk, and A. Lakhtakia, "Efficiency enhancement of ultrathin CIGS solar cells by optimal bandgap grading," *Appl. Opt.* **58**, 6067–6078 (2019).
13. F. Ahmad, T. H. Anderson, P. B. Monk, and A. Lakhtakia, "Efficiency enhancement of ultrathin CIGS solar cells by optimal bandgap grading: erratum," *Appl. Opt.* **59**, 2615 (2020).
14. H. Ferhati and F. Djeffal, "Graded band-gap engineering for increased efficiency in CZTS solar cells." *Opt. Mater.* **76**, 393–399 (2018).
15. F. Ahmad, A. Lakhtakia, T. H. Anderson, and P. B. Monk, "Towards highly efficient thin-film solar cells with a graded bandgap CZTSSe layer," *J. Phys. Energy* **2**, 025004 (2020).
16. F. Ahmad, A. Lakhtakia, T. H. Anderson, and P. B. Monk, "Corrigendum: Towards highly efficient thin-film solar cells with a graded bandgap CZTSSe layer," *J. Phys. Energy* **2**, 039501 (2020).
17. S. Amiri, S. Dehghani, and R. Safaiee, "Theoretical study of graded bandgap CZTSSe solar cells with two absorber layers," *Opt. Quantum Electron.* **52**, 323 (2020).
18. F. Ahmad, A. Lakhtakia, and P. B. Monk, "Optoelectronic modeling and optimization of graded-bandgap AlGaAs thin film solar cells," *Appl. Opt.* **59**, 1018–1027 (2020).
19. D.-K. Hwang, B.-S. Ko, D.-H. Jeon, J.-K. Kang, S.-J. Sung, K.-J. Yang, D. Nam, S. Cho, H. Cheong, and D.-H. Kim, "Single-step sulfo-selenization method for achieving low open circuit voltage deficit with band gap front-graded $Cu_2ZnSn(S,Se)_4$ thin films," *Solar Energy Mater. Solar Cells* **161**, 162–169 (2017).
20. L. M. Mansfield, A. Kanevce, S. P. Harvey, K. Bowers, C. Beall, S.

Glynn, and I. L. Repins, "Efficiency increased to 15.2% for ultra-thin Cu(In,Ga)Se_2 solar cells," *Prog. Photovolt.: Res. Appl.* **26**, 949–954 (2018).
21. J. F. Rasheed and V. S. Babu, "Performance evaluation of composition graded layer of a$Si_{1-x}Ge_x$:H in n^+aSi:H/i-aSi:H/p^+a$Si_{1-x}Ge_x$:H graded band gap single junction solar cells," *Mater. Today: Proc.* **27**, 26–31 (2020).
22. T. H. Anderson, B. J. Civiletti, P. B. Monk, and A. Lakhtakia, "Coupled optoelectronic simulation and optimization of thin-film photovoltaic solar cells," *J. Comput. Phys.* **407**, 109242 (2020).
23. T. H. Anderson, B. J. Civiletti, P. B. Monk, and A. Lakhtakia, "Corrigendum to 'Coupled optoelectronic simulation and optimization of thin-film photovoltaic solar cells' [J. Comput. Phys. 407 (2020) 109242]," *J. Comput. Phys.* **418**, 109561 (2020).
24. F. Ahmad, A. Lakhtakia, and P. B. Monk, *Theory of Graded-Bandgap Thin-Film Solar Cells* (Morgan & Claypool, 2021).
25. R. Storn and K. Price, "Differential evolution—a simple and efficient heuristic for global optimization over continuous spaces," *J. Glob. Optim.* **11**, 341–359 (1997).
26. D. W. Berreman, "Optics in stratified and anisotropic nedia: 4×4-matrix formulation," *J. Opt. Soc. Am.* **62**, 502–510 (1972).
27. T. G. Mackay and A. Lakhtakia, *The Transfer-Matrix Method in Electromagnetics and Optics* (Morgan & Claypool, 2020).
28. National Renewable Energy Laboratory, Reference Solar Spectral Irradiance: Air Mass 1.5 (accessed on June 9, 2021).
29. N. Vandamme, H.-L. Chen, A. Gaucher, B. Behaghel, A. Lemaître, A. Cattoni, C. Dupuis, N. Bardou, J.-F. Guillemoles, and S. Collin, "Ultrathin GaAs solar cells with a silver back mirror," *IEEE J. Photovolt.* **5**, 565–570 (2015).
30. J. Nelson, *The Physics of Solar Cells* (Imperial College Press, 2003).
31. D. Brinkman, K. Fellner, P. Markowich, and M.-T. Wolfram, "A drift-diffusion-reaction model for excitonic photovoltaic bilayers: Asymptotic analysis and a 2–D HDG finite-element scheme," *Math. Models Methods Appl. Sci.* **23**, 839–872 (2013).
32. B. Cockburn, J. Gopalakrishnan, and R. Lazarov, "Unified hybridization of discontinuous Galerkin, mixed, and continuous Galerkin methods for second order elliptic problems," *SIAM J. Numer. Anal.* **47**, 1319–1365 (2019).
33. G. Fu, W. Qiu, and W. Zhang, "An analysis of HDG methods for convection-dominated diffusion problems," *ESAIM: Math. Model. Numer. Anal.* **49**, 225–256 (2015).
34. M. J. Dodge, "Refractive properties of magnesium fluoride," *Appl. Opt.* **23**, 1980–1985 (1984).
35. N. Ehrmann and R. Reineke-Koch, "Ellipsometric studies on ZnO:Al thin films: Refinement of dispersion theories," *Thin Solid Films* **519**, 1475–1485 (2010).
36. C. Stelling, C. R. Singh, M. Karg, T. A. F. König, M. Thelakkat, and M. Retsch, "Plasmonic nanomeshes: their ambivalent role as transparent electrodes in organic solar cells," *Sci. Rep.* **7**, 42530 (2017).
37. R. E. Treharne, A. Seymour-Pierce, K. Durose, K. Hutchings, S, Roncallo, and D. Lane, "Optical design and fabrication of fully sputtered CdTe/CdS solar cells," *J. Phys.: Conf. Ser.* **286**, 012038 (2011).
38. R. Boidin, T. Halenkovič, V. Nazabal, L. Beneš, and P. Němec, "Pulsed laser deposited alumina thin films," *Ceramics Int.* **42**, 1177–1182 (2016).
39. M. R. Querry, "Optical constants of minerals and other materials from the millimeter to the ultraviolet," *Contractor Report* CRDEC-CR-88009, (1987) (accessed July 9, 2021).
40. S. Minoura, T. Maekawa, K. Kodera, A. Nakane, S. Niki, and H. Fujiwara, "Optical constants of Cu(In,Ga)Se_2 for arbitrary Cu and Ga compositions," *J. Appl. Phys.* **117**, 195703 (2015).
41. Y. Hirate, H. Tampo, S. Minoura, H. Kadowaki, A. Nakane, K. M. Kim, H. Shibata, S. Niki, and H. Fujiwara, "Dielectric functions of $Cu_2ZnSnSe_4$ and Cu_2SnSe_3 semiconductors," *J. Appl. Phys.* **117**, 015702 (2015).
42. A. Nakane, H. Tampo, M. Tamakoshi, S. Fujimoto, K. M. Kim, S. Kim, H. Shibata, S. Niki, and H. Fujiwara, "Quantitative determination of optical and recombination losses in thin-film photovoltaic devices based on external quantum efficiency analysis," *J. Appl. Phys.* **120**, 064505 (2016).
43. C. Frisk, C. Platzer-Björkman, J. Olsson, P. Szaniawski, J. T. Wätjen, V. Fjällström, P. Salomé, and M. Edoff, "Optimizing Ga-profiles for highly efficient Cu(In, Ga)Se_2 thin film solar cells in simple and complex defect models," *J. Phys. D: Appl. Phys.* **47**, 485104 (2014).
44. S. Adachi, *Earth-Abundant Materials for Solar Cells: Cu_2-II-IV-VI_4 Semiconductors* (Wiley, 2015).
45. A. Kanevce, I. Repins, and S. H. Wei, "Impact of bulk properties and local secondary phases on the $Cu_2ZnSn(S,Se)_4$ solar cells open-circuit voltage," *Sol. Energy Mater. Sol. Cells* **133**, 119–125 (2015).
46. E. N. Glytsis and T. K. Gaylord, "Rigorous three-dimensional coupled-wave diffraction analysis of single and cascaded anisotropic gratings," *J. Opt. Soc. Am. A* **4**, 2061–2080 (1987).
47. E. Ochoa-Martínez, L. Barrutia, M. Ochoa, E. Barrigón, I. García, I. Rey-Stolle, C. Algora, P. Basa, G. Kronome, and M. Gabás, "Refractive indexes and extinction coefficients of n- and p-type doped GaInP, AlInP and AlGaInP for multijunction solar cells." *Sol. Energy Mater. Sol. Cells* **174**, 388–396 (2018).
48. D. E. Aspnes, S. M. Kelso, R. A. Logan, and R. Bhat, "Optical properties of $Al_xGa_{1-x}As$," *J. Appl. Phys.* **60**, 754–767 (1986).
49. M. Schubert, V. Gottschalch, C. M. Herzinger, H. Yao H, P. G. Snyder, and J. A. Woollam, "Optical constants of $Ga_xIn_{1-x}P$ lattice matched to GaAs," *J. Appl. Phys.* **77**, 3416–3419 (1995).
50. P. B. Johnson and R. W. Christy, "Optical constants of the noble metals," *Phys. Rev. B* **6**, 4370–4379 (1972).
51. G. E. Jellison Jr., "Optical functions of GaAs, GaP, and Ge determined by two-channel polarization modulation ellipsometry," *Opt. Mater.* **1**, 151–160 (1992).
52. I. Vurgaftman, J. R. Meyer, and L. R. Ram-Mohan, "Band parameters for III–V compound semiconductors and their alloys," *J. Appl. Phys.* **89** 5815–5875 (2001).
53. A. S. Gudovskikh, N. A. Kaluzhniy, V. M. Lantratov, S. A. Mintairov, M. Z. Shvarts, and V. M. Andreev, "Numerical modelling of GaInP solar cells with AlInP and AlGaAs windows," *Thin Solid Films* **516**, 6739–6743 (2008).
54. S. Adachi, "GaAs, AlAs, and $Al_xGa_{1-x}As$: Material parameters for use in research and device applications," *J. Appl. Phys.* **58**, R1–R29 (1985).
55. S. Adachi (ed), *Properties of Aluminum Gallium Arsenide*, EMIS Datareviews Series No. 7 (INSPEC, Institution of Electrical Engineers, London, UK, 1993).
56. Ioffe Institute, $Al_xGa_{1-x}As$ (accessed on October 26, 2021).
57. F. Ahmad, T. H. Anderson, B. J. Civiletti, P. B. Monk, and A. Lakhtakia, "On optical-absorption peaks in a nonhomogeneous thin-film solar cell with a two-dimensional periodically corrugated metallic backreflector," *J. Nanophotonics* **12**, 016017 (2018).